Primate cathelicidin orthologues display different structures and membrane interactions

Francesca Morgera, Lisa Vaccari, Nikolinka Antcheva, Denis Scaini, Sabrina Pacor, Alessandro Tossi

Primate cathelicidin orthologues display different structures and membrane interactions

Francesca Morgera*,†, Lisa Vaccari†, Nikolinka Antcheva*, Denis Scaini†, Sabrina Pacor*, Alessandro Tossi*

*Department of Life Sciences, University of Trieste, 34127 Trieste, Italy

† Elettra Synchrotron Light Laboratory, 34012 Basovizza, Trieste, Italy

correspondence to : F. Morgera (francesca.morgera@elettra.trieste.it)

The human cathelicidin LL-37 displays both direct antibacterial activities and the capacity to modulate host cell activities. These depend on structural characteristics that are subject to positive selection for variation, as observed in a previous analysis of the *CAMP* gene in primates. The altered balance between cationic and anionic residues in different primate orthologues affects intramolecular salt-bridging and influences the stability of the peptides' helical conformation and tendency to aggregate in solution. We have analysed the effects of these structural variations on membrane interactions for human LL-37, rhesus RL-37, and orang-utan LL-37, using several complementary biophysical and biochemical methods. CD and ATR-FTIR spectroscopy on model membranes indicate that RL-37, which is monomeric and unstructured in bulk solution (F-form), and human LL-37, which is partly structured and likely aggregated (A-form), bind biological membranes in different manners. RL-37 may insert more deeply into the lipid bilayer than LL-37, which remains aggregated. AFM performed on the same supported bilayer as used for ATR-FTIR measurements suggests a carpet-like mode of permeabilization for RL37 and formation of more defined worm-holes for LL-37. Comparison of data from biological activity on bacterial cells with permeabilization of model membranes indicates that the structure/aggregation state also affects the trajectory of the peptides from bulk solution through the outer cell-wall layers to the membrane. Our data suggests that F-Form cathelicidin orthologues may have evolved to have primarily a direct antimicrobial defensive capacity while A-form ones have somewhat sacrificed this to gain host-cell modulating functions.

Short title: Membrane interaction of primate Cathelicidin orthologues

Key words: antimicrobial peptides, primate Cathelicidin, peptide structuring, membrane interaction, mode of action, ATR spectroscopy.

Abbreviations used: LUV, large unilamellar vesicles; PG, phosphatidyl-DL-glycerol; DPG, di-phosphatidyl-DL-glycerol; PC, L-α-phosphatidylcholine; SM, sphingomyelin ; Ch, cholesterol; TFE, trifluoroethanol; PBS, sodium phosphate buffer; TSB, triptic soy broth; ATR, attenuated total reflection; AFM, atomic force microscopy; ANTS, 8-amino-naphtalene-1,3,6 trisulfonic acid; DPX, p-xylene-bys-pyridinium bromide; PI, propidium iodide; DiBAC, bis-(1,3-dibarbituric acid)-trimethine oxanol; MIC, minimum inhibitory concentration; FDG, fluorescein-di-β-D-galactopyranoside.

INTRODUCTION

The human helical peptide LL-37 displays unique properties amongst antimicrobial peptides (AMPs). It has acquired structural and functional properties that distinguish it from the numerous other reported helical AMPs, produced by organisms ranging from bacteria to insects, amphibians, fish and other mammals [1], and is an extraordinary example of how evolution can find new functions for ancient molecules within the context of the ongoing struggle between host and pathogen.

Antimicrobial *host defence peptides* (HDPs) such as LL-37 have multiple functions in immunity, combining a direct antimicrobial activity with the capacity to act on host immune cells, a role at the interface between the innate and adaptive defence systems that makes them important immune effectors and potentially valuable tools for treating infection [2]. The cathelicidin family of HDPs, to which it belongs, is characterized by well conserved, cathelin-like pro-regions from which individual, structurally diverse, C-terminal antimicrobial peptides are released after proteolytic cleavage [3]. It is ubiquitously found in mammals, from marsupials to glires, bovids, pigs, horses, dogs and primates, and may play similar roles also in other vertebrates such as amphibians and fish. However, while multiple structurally different cathelicidins are present in some animals (e.g. in artiodactyl species, for example), only one helical peptide is produced by primates, including humans.

LL-37 is encoded by the *CAMP* gene, and is expressed as the propeptide hCAP-18. It was first identified in neutrophils [4] and later in various epithelial and inflammatory cells [5-7]. The 37 residue C-terminal AMP domain becomes active after release from CAP-18 by proteinase 3 [8], and its first line role in host defence is supported by the fact that it has been identified in leukocytes and mast cells, as well as a large variety of epithelial tissues, and that it is released into body fluids such as airway, seminal and amniotic fluids, plasma and wound secretions [9]. Its release is mediated by pro-inflammatory stimuli and it can then exert a membrane-directed, broad-spectrum antimicrobial activity *in vitro* [3,10] that is sensitive to both salt concentrations and serum components, albeit in a different manner to the defensins [11]. This is accompanied by some *in vitro* cytotoxicity towards host cells, indicating a capacity to interact with their membranes also [12-14]. At non-cytotoxic concentrations, LL-37 has been variously reported to display other activities related to host defence and healing, such as chemotaxis of T-cells, leukocytes and neutrophils, or stimulation of cell proliferation and angiogenesis, requiring interaction with specific membrane-bound receptors such as the formyl peptide receptor like 1 (FPRL-1) [15-16] and the epidermal growth factor receptor (EGFR) [17].

All these diverse activities of LL-37 are packed into a small, deceptively simple structure; the amphipathic, α-helical conformation displayed by many other AMPs [1], and all likely require interaction with biological membranes at some point. LL-37, however, sets itself aside from this structural group of AMPs in significant ways. It is characterized by a high content of both cationic and anionic residues (16 out of 37 leading to a net charge +6 at physiological pH) that allows the formation of an extensive network of intramolecular salt bridges, and permits the formation of a stable helical conformation in aqueous solution in a concentration and salt dependent manner [12,14]. Most other helical AMPs can only acquire such a conformation in the presence of biological membranes, by virtue of the amphipathic residue arrangement. This structural characteristic of LL-37 appears to be an evolutionarily selected trait that has strong implications on its aggregational properties, or on how it interacts with extracellular fluid components or the membrane itself [12,18,19], and so modulates its functions.

A recent analysis of numerous orthologues of the *CAMP* gene in non-human primates indicates that the region coding for the mature peptide is subject to positive selection for variation. In particular, it affects the net charge (which ranges from +4 to +11 in different primate orthologs), without significantly affecting the overall hydrophobicity and amphipaticity of the encoded peptides [14].

This is achieved by altering the proportion of basic, neutral and acidic residues in its polar sector, thus also altering the salt-bridging pattern and strongly influencing the structural/aggregational behaviour of different primate orthologs. In turn, this affects their approach and insertion modes at the membrane surface, leading to diverse biological effects on eukaryotic and prokaryotic cells. The observed variations may thus influence the subtle balance existing between direct antimicrobial activities, cytotoxicity, receptor-mediated immuno-modulatory effects, and the tendency to interact with extracellular fluid components. All this underlines the need for a systematic approach to the investigation of the differential modes of action of LL-37 homologues, in which the structural requirements for the various activities are somehow dissected. In this context, a detailed study of how structural variations affect peptide-membrane interactions (following the approach-binding-insertion trajectory), appears a necessary step. We have made use of several complementary biophysical and biochemical methods to systematically examine the effects of structural variations and attempt to relate them to different aspects of LL-37's mode of action.

MATERIALS AND METHODS

Peptide synthesis and characterisation. Fmoc-solid phase peptide synthesises were performed on either Pioneer® (PE Biosystems) peptide synthesizer, following a protocol described previously [14]. Peptides were cleaved from the resin with a version of the reagent K and then the crude peptide was purified with a Waters Delta Pak® C_{18} column (5μm, 300 A°, 25 mm x 100 mm). The quality and correctness of the peptides was confirmed using ESI-MS (Bruker Esquire 4000). Peptide solutions were prepared from stock solutions in water, in which their concentrations were independently quantified by i) the weight of the peptide used, ii) colorimetric determinations using the bicinconinic acid method (Pierce, Rockford IL), iii) Phe absorption at 257 nm (ε_{257}=195.1).

Preparation of liposomes. LUVs were prepared by extrusion of anionic PG/dPG (95:5, w/w, from egg yolk lecithin and bovine heart respectively). Zwitterionic LUVs were prepared using PC/SM/Ch (40:40:20, w/w) dispersions (phospholipids from chicken egg yolk). All components were purchased from Sigma Aldrich. Dry lipids were dissolved in chloroform, evaporated under a stream of nitrogen and the residue vacuum-dried for 3 h. The lipid cake was resuspended to a concentration of 3 mg/ml in the appropriate buffer by spinning the flask at a temperature above the Tc. The resulting multilamellar vesicle suspensions were disrupted by several freeze-thaw cycles prior to extrusion with a Mini-Extruder (Avanti Polar Lipids, Inc.) through polycarbonate filters with 100 nm pores. LUVs were freshly prepared and used within one or two days.

Circular Dichroism. CD spectroscopy was performed on a J-715 spectropolarimeter (JASCO Corp. Japan), using 2-mm quartz cells and 20 μM peptide with or without phospholipid vesicles (0.4 mM phospholipids) in 0.150 M NaCl and 0.010 M sodium phosphate (PBS buffer) at pH 7.0 and room temperature. Peptide/lipid suspensions (molar ratio 1:20) were incubated for 30 min. at 37 °C before use. Spectra are the average for at least two independent experiments, each with accumulation of three scans.

Transmission FTIR. Spectra (512 scans, spectral resolution 2 cm^{-1}) were collected with Vertex 70 Bruker interferometer, using 2 mM peptide solutions in D_2O placed between CaF_2 windows, spaced 25 microns apart in a dismountable liquid cell (Harrick Scientific Products, Inc.), after allowing the amide II band to shift from 1550 to 1460 cm^{-1} to ensure complete deuterium exchange. Nonlinear least-square curve fitting with Gaussians bands was used to identify the components of the amide I band. Starting parameters for the fitting process were obtained by Second-derivative spectra (9-data-point Savitzky-Golay algorithm).

ATR-FTIR. ATR-FTIR. Spectra were collected with the HORIZON™ multiple reflectance ATR accessory (Harrick Scientific Products, Inc.) mounted on a Bruker Vertex 70 FTIR spectrometer equipped with a Mid Band Mercury-Cadmium-Telluride detector (MCT D316), by acquiring 128

scans with a resolution of 4 cm^{-1}. Supported lipid multibilayers are obtained by means of the spinning method [20]. In brief, pure PG lipid (10 mg/ml), dissolved in chloroform, was directly pipetted onto a clean Germanium crystal (50 mm x 10 mm x 2 mm), which was then accelerated to rotation of 2000 rpm, for 2 minutes, using a spin-coater, and then vacuum-dried for 3 h. This procedure resulted in relatively homogeneous and ordered multibilayers of about 50 nm thickness (≈ 10 bilayers), as confirmed by AFM performed directly on the crystal (data not shown), and further backed by IR spectra. The crystal was then placed into a customized sealed ATR cell and hydrated by first increasing the relative humidity of the system and then by coating it with a thin aqueous film. In presence of water the lipid film exfoliates by giving rise to vesicles, leaving only one or two bilayers on the crystal, as confirmed by AFM and by a 10-fold decrease in IR absorbance. Peptide solution was then injected onto the hydrated multibilayers. After 1h, unbound peptide was gently washed out and the spectrum of the only dried membrane-bound peptide was recorded. The background was collected directly on a clean internal reflection element (IRE). Any contribution of water vapour to the absorbance spectra in the amide I peak region was corrected by spectral subtraction.

In order to obtain an estimate of the peptide/lipid molar ratio, ATR-FTIR spectra of peptide-lipid multibilayers were also recorded at different known peptide concentrations, following the method of Bechinger and co workers [21]. For multibilayers thinner than the penetration depth of evanescent field, as those used in this experiment, a direct comparison of the amide I/acyl chain integral ratio could be calculated, allowing a final peptide/lipid ratio estimation of about 1:20.

AFM Characterization

Dried PG bilayers, supported on the ATR crystal, obtained as described above, were previously characterized before and after exfoliation by successive hydration/surface washing cycles, to ensure single bilayer formation. The dried bilayers were then morphologically characterized immediately before hydration and use in IR experiments, and then after peptide addition and dehydration, using a Solver PRO AFM instrument (NT-MDT Co., Moscow). Topographic and phase images were acquired in semi-contact mode [22] using golden-silicon AFM tips (NT-MDT Co., NSG10 rectangular cantilevers, spring constant 11.5 N/m, resonant frequency 255 kHz, probe tip radius 10 nm). All measurements were carried out under atmospheric conditions.

Dye release from ANTX/DPX pre-loaded liposomes. LUVs were prepared as previously. Briefly, the lipid cake was resuspended in PBS buffer in which the dye/quencher pair ANTS/DPX [23] (9mM/25mM, Molecular Probes) were dissolved. After extrusion through polycarbonate filter, free dye was removed using a Sephadex G-75 gel filtration column, eluting with PBS. Fluorimetric analyses were carried on 96 well plates, with varying peptide concentrations (1, 5, 10, 20 μM). LUVs were added to wells containing peptide solutions, to a final lipid concentration of 300 μM in each well, and fluorescence then monitored continuously over time on a Hidex Chameleon reader, (λ_{ex} = 360 nm, λ_{em} = 515 nm). LUVs added to wells containing 0.2% TritonX-100 solution (100% disruption) or just buffer (no disruption) were respectively used as positive (maximal fluorescence-f_{max}) and negative (minimal fluorescence-f_0) controls. 0,2% Triton X-100 was also added to peptide-containing and negative control wells at the end of the time-course, to obtain full dye release. The fluorescence intensities were subsequently corrected for both background and dilution and data are reported as fractional fluorescence, according to the formula: $f^{frac} = (f-f_0)/(f_{max}-f_0)$. Results are the mean of at least three independent experiments run in triplicate.

Antimicrobial and cell permeabilising activities.

The concentration and medium dependent antimicrobial activities of the peptides was qualitatively evaluated by following the inhibition of bacterial growth by peptides for 10^6 CFU/ml *E.coli* ML35 or *S.aureus* 710A cells placed in a 96 well plate under different medium conditions and peptide concentrations (5%, 20% or 50% TSB in 0.010 M phosphate buffer (SPB); 0.5, 1 or 5 μM peptide). Growth was monitored at 600 nm for 4 hours at 37°C, with a Tecan Sunrise reader. Plates were then incubated overnight to determine if long-term growth inhibition occurred, by visual inspection.

Permeabilization of single *E.coli* cells was evaluated by following propidium iodide (PI) uptake by flow cytometry. Suspensions of 10^6 CFU *E.coli* ML35 in PBS were exposed to 0,1 μM of the desired peptide, and after 4 minute of incubation with PI (10 μg/ml) at 37 °C, PI fluorescence was followed for 40 min. Fluorescence data from cells showing permeability to PI were acquired in a monoparametric histogram (emission wavelength, 612 nm), using a Cytomics FC 5000 flow cytometer (Beckman Coulter, Inc., Fullerton, CA), equipped with an Argon laser (488 nm, 5 mW), supported by forward and side light scatter detectors and five PMT fluorescence detectors. Histograms were analyzed with the WinMDI software (Dr J. Trotter, Scripps Research Institute, La Jolla, CA, U.S.A.). The effect on bacterial transmembrane potential was evaluated under the same conditions by using DiBAC4(3), adding it to a final concentration of 1 μM. Samples were then analyzed after 4 min of incubation at 37°C, as described for PI. All the dyes were purchased from Molecular Probes.

RESULTS

Three LL-37 orthologues were selected for this investigation, so as to explore the role of structural/aggregational behaviour on biological activities. Johansson and co-workers have previously investigated the capacity of LL-37 to structure under various solution conditions, highlighting that the helical conformation is accompanied by aggregation in a manner that is highly dependent on the presence of physiologically relevant ions and membrane-like environments [12]. In this study this peptide was compared to the *Rhesus macaque* orthologue *mmu*RL-37 and the orang-utan orthologue *ppy*LL-37. The macaque peptide has a higher cationic residue content, resulting in a higher charge (+8) than human LL-37 (+6), and in an excess of charged side-chain repulsions than attractions when the helix forms (Table 1)[14], so that it is unstructured and likely monomeric in bulk solution. Conversely, *ppy*LL-37 has the lowest charge (+4) amongst analyzed orthologues and the highest number of interhelix electrostatic attractions with respect to repulsions, which should stabilize this structure (Table 1). The different structuring and aggregational properties of the peptides affect their antimicrobial activity as well as their mode of interaction with biological membranes [14].

Peptide structure characterization in solution or in the presence of biological membranes – Structuring of the three peptides was studied i) by CD spectroscopy both in aqueous solutions and in the presence of anionic and zwitterionic liposomes; ii) by means of Fourier Transformed Infrared (FTIR) transmission spectroscopy in concentrated D_2O solutions; and iii) by means of ATR-FTIR on supported hydrated or dehydrated lipid bilayers. These spectroscopic approaches are complementary, allowing structure assessment in a wide peptide concentration range (micromolar to millimolar), display different sensitivities to conformational components, and can provide different types of information on the aggregational state.CD spectroscopy indicates that the three peptides behave differently in aqueous buffer. In PBS (Fig. 1), *ppy*LL-37 has a greater helical content (> 65%) than LL-37 (~ 30%), or *mmu*RL-37 (< 5%), estimated by Chen's method [24], while they all show a comparably high helical content (65-75%) in 50% TFE This indicates that *ppy*LL-37 is substantially structured/aggregated and *mmu*RL-37 unstructured/monomeric in aqueous buffer, while LL-37 is either in equilibrium between these two states, or adopts an aggregational form which is only partially helical.

CD spectra in the presence of anionic and neutral liposomes, used to respectively model bacterial and eukaryotic membranes, are also quite revealing. All three peptides show helix-type spectra in the presence of PG/dPG LUVs (Fig.1), similar to those observed in TFE, indicating that they interact in a fully structured form, with this type of membrane. Conversely, spectra in the presence of neutral LUVs are more similar to those observed in saline buffer, indicating either a lack of interaction with zwitterionic membranes, or one that does not result in significant structural variations. In this respect, it is useful to also consider variations in the shapes of spectra in the presence of LUVs. Lau et al. have reported that the $[\theta]^{222}/[\theta]^{208}$ ratio between the ellipticity minima for helical segments can provide

information on their aggregation, being <1 for lone helices and ≥ 1 for stacked helices [25]. The ratio is in fact <1 for all three AMPs in TFE, compatible with a monomeric helical state, and *mmu*RL37 continues to maintain this ratio also in the presence of anionic PG/dPG LUVs (Fig.1B), so it doesn't appear to aggregate upon membrane interaction. Orang-utan and human LL-37 instead show a peak ratio ≈ 1 in both saline buffer and in the presence of anionic LUVs, compatible with a more aggregated state. In the presence of neutral LUVs they switch to a peak ratio visibly greater than 1, suggesting that interaction with such membranes may accentuate this state (Fig.1A&C).

FTIR transmission spectroscopy in deuterated water was carried out at higher concentrations (2 mM), which may reflect those attained at the bacterial surface due to pseudo-concentration effects. Spectra of LL-37 (Fig.2A-1,2), after complete H/D exchange, indicate a stable helical structure, so that high concentration favours structuring by aggregation, even in the absence of salt. *mmu*RL37 instead shows a broader, more composite amide I band (see fig.2-B1 and second derivative in 2-B2), indicative of a more random structure even under these high concentration conditions. Side chain contributions from Arg residues [26-28] are also evident for both peptides (symmetric and antisymmetric stretching modes at 1608 and 1585 cm^{-1} respectively; Fig.2-A, B2).

Peptide structure in the presence of supported membrane – Peptide secondary structure in the presence of a PG bilayer supported on a germanium crystal, a simple model for bacterial membranes with which all three orthologues appear to interact strongly, was investigated by ATR-FTIR. This technique also provided information on peptide effects on the lipid order upon interaction. The ATR experiment was combined with atomic force microscopy (AFM) in tapping mode, carried out directly on the same ATR crystal supported bilayers, to provide both confirmation of the quality of the supported membrane and some insight on the morphological state of the bilayers before and after the peptide insertion (Fig.5), contributing to a more complete description of the peptide-membrane interaction.

Fig.3A shows the part of the ATR-FTIR spectrum pertinent to the peptide amide I and II absorptions, for LL-37 in contact with the bilayer after dehydration, revealing a sharp band centred at 1652 cm^{-1}, typically assigned to an α-helical structure [29]. Two other components at 1630 and 1683 cm^{-1} (Fig. 3A-2) were assigned to arginine side chains participating in salt bridges they give rise to a specific CN stretching frequencies (symmetric and antisymmetric stretching modes respectively). These bands are reported to red-shift in a non polar environment [30].

For *mmu*RL37, ATR amide I and II bands (Fig.3B) also show a strong α-helical signal (1656 cm^{-1}) which is significantly red-shifted with respect to LL-37, possibly indicating a deeper insertion into the hydrophobic environment of the membrane [31]. Consistent with this hypothesis, the CH_2 stretching frequencies of the lipid acyl bands (at 2920 and 2850 cm^{-1} for the antisymmetric and symmetric modes respectively) shift and broaden more on insertion of *mmu*RL-37 (to 2924 and 2854 cm^{-1} Fig.4B) than LL-37 (2922 cm^{-1} and 2852 cm^{-1}, Fig. 4A), suggesting a greater effect of RL-37 on the lipid order [32].

AFM images of dehydrated PG bilayers before and after exposure to either peptide are shown in Fig. 5 add to the indications they interact with and alter the anionic membrane in a different manner. *mmu*RL37 seems to cause a generalized perturbation in the bilayer, resulting in lesions of varying sizes (Fig.5-C1) and with a more amorphous appearance. LL-37 instead generates a more defined pattern of perturbations consistent with the formation of many holes of roughly the same size (about 10 nm) that are visible only at higher resolution (Fig.5-B1 and inset). Their topography is characterized by a positive curvature suggesting that accumulation of AMPs at the bilayer surface may facilitate the bending of phospholipids into a wormhole or toroidal pore [33-34]. The hole size is larger than previously reported for such pores formed by other AMPs (3-5 nm) using other methods [35-36], but this may in part be ascribed to convolution effects deriving from the size of the AFM tip, leading to an overestimation. AFM-phase imaging provides information on physical variations beyond morphology, and indicates that the lipid bilayer preserves its phase homogeneity upon LL-37

interaction (Fig.5-B2), while it becomes inhomogeneous upon *mmu*RL37 interaction (Fig.5-C2). This is consistent with an important perturbation of the lipid order induced by *mmu*RL-37, which less appreciable for the human peptide (Fig.5-B1, 2 insets). Our conclusions are in qualitative agreement with solid state ^{31}P-NMR and differential scanning calorimetry that indicate a concentration-dependent positive curvature strain induced by LL-37 to anionic lipid bilayers, consistent with a toroidal pore model [37]. *mmu*RL-37 may instead act by a more carpet-like mechanism at similar concentrations.

Permeabilization of model and bacterial membranes – The behaviour of LL-37 orthologues in the presence of model membranes was correlated to their permeabilizing effects on both model and real membrane systems. In the first case, the same type of anionic and zwitterionic LUVs used for CD spectroscopy were pre-loaded with the ANTS/DPX fluorescent dye/quencher pair. Dye release kinetics were then monitored in presence of the peptides at different concentrations. As shown in fig.6, at lower concentrations *ppy*LL-37 resulted in the most efficient dye release for both anionic PG/dPG and zwitterionic PC/SM/Ch LUVs, followed by LL-37 and then *mmu*RL-37, whereas at higher peptide-lipid ratios all the peptides resulted in ≈ 80-90% leakage from both. It is interesting that *mmu*RL-37 displays a significant capacity to permeabilise zwitterionic vesicles even though it does not structure in their presence (Fig.6B and Fig.1B). Zwitterionic LUVs were more prone to fusion than the anionic ones and were efficiently induced to fuse or aggregate at by both peptides (results not shown), which may provide a possible means of dye release [23].

The effect of the peptides on bacterial membranes was monitored by following both the permeabilization of a population of *E. coli* ML-35 cells, and the depolarization of their membranes by means of flow cytometry (Fig.7A). Membrane lysis, assessed by following PI fluorescence, followed a diametrically opposite trend to that observed for dye release from anionic LUVs, with permeabilization efficiencies following the order *mmu*RL-37 > human LL-37 > *ppy*LL-37, so that the processes governing lysis of naked model membranes are clearly different to those that apply to bacterial cells. This trend was substantially confirmed also in steady state fluorescence assays using the fluorogenic or chromogenic β-galactosidase substrates FDG and ONPG [38](results not shown). Moreover, at specific times, *E.coli* cells were stained with the transmembrane potential probe DiBAC4(3), allowing the simultaneous detection and temporal discrimination of depolarized cells and PI permeabilized cells (Fig.7-B1,B2).

In particular, *mmu*RL37 permeabilized 23% of the *E.coli* cell population after only 10 minutes, reaching 85% PI-positive cells after 40 minutes exposure (Fig.7A). This effect is preceded by a substantial and very rapid depolarization of the bacterial membranes, observable on the whole population after just 4 minutes exposure and then remaining constant during the time course of the experiment, as showed by DiBAC fluorescence in Fig.7 -B1&2. LL-37 causes a slower albeit still quite efficient permeabilization on the selected bacterial cells (28% PI-positive cells after 20 min, 62% after 40 min), and in this case depolarization may accompany rather than precede the primary permeabilising effect, as DiBAC-positive cells are significant only at 30 minutes exposure. *ppy*LL-37 exerted a negligible effect on both permeabilization and depolarization of the *E.coli* cell population, under these conditions, within the time-scale of the experiment.

The question remained as to whether these opposite trends derive from effective differences in real and model membrane compositions, or are rather due to the presence of other cell wall and/or medium components in assays with bacterial cells. We had previously observed a dependence of MIC values for LL-37 orthologues on medium composition [14], and confirmed this by observing the effect of the three peptides on bacterial growth kinetics, at different concentrations, and in different medium conditions (results not shown). Both human and orang-utan LL-37 lost activity on changing from 5% to 50% TSB while *mmu*RL-37 did not (results not shown). It was also more efficient at inhibiting the growth of *S. aureus*, under low medium conditions, than the LL-37 orthologues. We previously reported lower MIC, faster killing and faster membrane permeabilisation of gram-positive bacteria for *mmu*RL-37 and a similarly unstructured orthologue, *prespytis obscura* RL-37 (charge +10), than for

human LL-37 and similarly structuring orthologues [14]. This has been ascribed to the former peptides being better able to penetrate and bypass the thick peptidoglycan layer.

DISCUSSION

The approach-binding-insertion trajectory of AMPs is affected by their aggregational behaviour and sequential interactions with multiple medium or cell wall components, as schematically shown fig.8. From the extracellular aqueous medium (layer A), they must cross the outer cell-wall (layer B) to interact with cytoplasmic membrane (layer C) and possibly translocate into the cytoplasm (layer D). They can be monomeric and unstructured in bulk solution (free or F-form) or in equilibrium with stable conformational (1) and aggregational (2) forms (A-form), and can bind non-productively to medium, serum or interstitial components or bacterial exopolisaccharides (3) [18-19] (segregated or S-form). Their subsequent activities are modulated by how each of these forms interact with outer membrane (e.g. LPS), or cell wall (peptidoglycan or teichoic acid) components (4), as well as how they insert into the cytoplasmic membrane bilayer.

Bacterial inactivation has then been postulated to occur by one or more of several possible mechanisms, including formation of a generalized membrane surface disruption as described by the "carpet" or "aggregate channel" mechanisms (6) and formation of transient "toroidal or worm-hole" pores (7) (combined in the Shai-Matzusaki-Huang model) [39]. Surface interaction with, or insertion into the membrane would also likely lead to interference with vital membrane-located protein machinery, as conceptualized in the "sand-in-a-gearbox" model (8) [40]. Should the peptides translocate across the membrane, they could also interfere with vital cytoplasmic components (e.g. proteins and/or DNA)(9). It is within this conceptual framework that we have planned, executed and interpreted our experiments to probe the mode of action of LL-37 and its orthologues.

Our data indicate that while *mmu*RL-37 exists primarily in the unstructured monomeric F-form in physiological solutions, *ppy*LL-37 has a helical structure, stabilized by the formation of intramolecular salt-bridges, and is likely in the A-form, as suggested by an $[\theta]^{222}/[\theta]^{208}$ ratio ≈ 1 observed in CD spectra. Human LL-37 seems to assume an intermediate, partially structured form, and/or may be in a salt and concentration dependent equilibrium between the F- and A-forms [(1) in Fig.8, layer A]. These conclusions are backed both by CD spectroscopy in aqueous buffer and transmission FTIR. The NMR structure of LL-37 in DPC micelles has recently been reported, and in fact shows a helix-break-helix conformation with unstructured N- and C- termini [41]. CD spectra in the presence of anionic membranes indicate that human and orangutan LL-37 may interact with these in the aggregated form, whereas *mmu*RL-37 structures and binds as a monomeric helix. Furthermore, the lack of structuring for *mmu*RL-37 and altered $[\theta]^{222}/[\theta]^{208}$ ratio for human or *ppy*LL-37 in the presence of neutral LUVs, may indicate a selective capacity of A-form peptides to bind to zwitterionic membrane in a manner that enhances stacking. The fact that peak intensities do not change with respect to saline buffer may be in line with a more surface type interaction that does not greatly alter the conformational stability. These observations could be quite relevant to capacity of LL-37 to modulate host cells. It has in fact recently been reported that LL-37 and other A-form orthologues, including *ppy*LL-37, can induce fibroblast proliferation, acting through receptor P2X7, whereas the macaque and *Presbytis obsucura* RL-37 F-form orthologues were inactive [42].

ATR-FTIR experiments in the presence of supported PG bilayers suggest a deeper insertion of *mmu*RL-37 into the lipid bilayer than LL-37, and a more disruptive effect on the membrane order. An explanation could be that *mmu*RL-37 sinks more deeply into the lipid layer as a log-like monomeric helix, also by virtue of the so-called 'snorkel' effect, while LL-37 may remain more on the surface as a helical bundle. We have shown previously, using model helical peptides, that the 'snorkel' effect can have a considerable impact on their capacity to permeabilise biological membranes [43]. An intimate association with the membrane surface is also demonstrated by red-shifts in specific CN and COO^- stretching frequencies that have been associated with Arg residues salt-bridging in a less

hydrated environment [30]. Different modes of interaction with, and insertion into, the bacterial surface are likely to affect the subsequent modes of membrane permeabilisation [Fig 8. (5-9)], and AFM performed on the same supported bilayer as used in ATR-FTIR strongly supports this hypothesis. In the presence of *mmu*RL-37, the morphology of the membrane suggests larger and heterogeneous surface lesions compatible with the carpet mechanism, while for LL-37 smaller discrete perforations are evident, more in agreement with the formation of worm-holes.

The use of fluorophore/quencher loaded anionic or neutral liposomes in the presence of the peptides was used to further study these potentially different membrane permeabilising effects. Under the conditions used, however, all three peptides efficiently resulted in release not only from anionic LUVs, but also neutral ones. Formation of a helical structure was thus not a prerequisite for exerting an efficient lytic activity on naked zwitterionic membranes, although dye release in this case may also derive from mechanisms related to the induction of liposome aggregation or fusion [23]. The fact that dye release from anionic LUVs was similar for the three peptides, whereas antimicrobial activity and bacterial membrane permeabilisation were not, indicated that their biological activity was not just a consequence of membrane lysis. *mmu*RL-37 displayed the overall most potent antimicrobial activity *in vitro*, covering both Gram-positive and Gram-negative bacteria, and a better capacity to permeabilise a bacterial membrane, with a significantly lower medium/salt sensitivity, than human or orang-utan LL-37. Part of the explanation seems to be a lower tendency of the F-form macaque peptide to bind to medium components, than the A-form, thus avoiding the less active S-form [Fig. 8 (3)]. LL-37 peptides, apart from being more subject to converting to the S-form, may also interact more strongly with outer cell wall components such as the peptidoglycan (Fig. 8 [4]) explaining their relatively lower activity against *S. aureus*. The requirements for efficiently approaching the membrane, from bulk solution through the outer cell-wall layers to the membrane surface itself, are therefore different to those for membrane insertion and lysis, and the former may dominate in deciding the antimicrobial potency.

Flow cytometric experiments in which two effects of membrane damage, permeabilisation to propidium iodide and membrane depolarisation, were measured concurrently, indicate that *mmu*RL-37 results in a very rapid depolarisation and efficient permeabilisation of the bacterial membrane. LL-37 acts more slowly, though permeabilisation is comparable on the long term, and depolarisation seems concurrent to it. These data are compatible with a detergent-like carpet mechanism for the macaque peptide and pore formation for the human one, and relate to different killing efficiencies, but it should be considered that membrane disruption is only one factor contributing to cellular inactivation. Other concurrent factors need to be taken into account, such as interference with essential membrane-bound proteic complexes [as proposed by the 'sand-in-a-gearbox' mechanism, Fig 8 (8)] or translocation to cytoplasmic targets [Fig. 8 (9)], which may also be carried out in different manners by the two types of peptides.

In conclusion, it would appear that the evolution of the primate cathelicidin has led to sequence variations that have resulted in distinct structuring capacities for different orthologues, which in turn result in different modes of membrane interaction that cause different types of membrane lesions. In particular, some primate orthologues behave like many other helical AMPs from vertebrate and invertebrate animals that are random-coil in physiological solution and structure only at the bacterial surface. This ensures a potent, broad-spectrum activity *in vitro* that is relatively insensitive to medium or salt effects, appears to allow a more efficient penetration across external cell wall components, and ultimately results in membrane damage predominantly by a carpet-like mechanism. Other orthologues, including the human one, have gained a salt-dependent capacity to structure in saline solutions, which leads to aggregation and a greater tendency to stick to medium (and possibly also to serum and bacterial cell-wall) components, in a manner that apparently reduces their direct antimicrobial potency. This may however be compensated by a better capacity to interact in a productive manner with eukaryotic membranes [42], in agreement with the many reported activities of human LL-37 on host immune cells. It is tempting to speculate that F-Form primate cathelicidin

orthologues have evolved to have primarily a directly antimicrobial defensive capacity, while A-form ones have somewhat sacrificed this to gain in host-cell modulating functions.

ACKNOWLEDGMENTS

This study was supported by grants from the Italian Ministry for University and Research (PRIN 2005), by the EU VIth framework project ETPA (COOP-CT-2005-018191) and by FVG LR11/2003 and 26/2005 projects. F. Morgera is supported by an Elettra Ph.D grant.

REFERENCES

1 Tossi, A., Sandri, L. and Giangaspero, A. (2000) Amphipathic, alpha-helical antimicrobial peptides. Biopolymers **55,** 4-30

2 Hancock, R.E. and Sahl, H.G. (2006) Antimicrobial and host-defense peptides as new anti-infective therapeutic strategies. Nat Biotechnol **24**, 1551-1557

3 Zanetti, M. (2004) Cathelicidins, multifunctional peptides of the innate immunity. J Leukoc. Biol. **75**, 39-48

4 Sørensen, O., Arnljots, K., Cowland, J. B., Bainton, D. F. and Borregaard, N. (1997) The human antibacterial cathelicidin, hCAP-18, is synthesized in myelocytes and metamyelocytes and localized to specific granules in neutrophils. Blood **90**, 2796-2803

5 Frohm, N. M., Sandstedt, B., Sørensen, O., Weber, G. Borregaard, N. and Stahle-Backdahl, M. (1999) The human cationic antimicrobial protein (hCAP18), a peptide antibiotic, is widely expressed in human squamous epithelia and colocalizes with interleukin-6. Infect. Immun. **67**, 2561-2566

6 Bals, R., Wang, X., Zasloff, M. and Wilson, J. M. (1998) The peptide antibiotic LL-37/hCAP-18 is expressed in epithelia of the human lung where it has broad antimicrobial activity at the airway surface. Proc. Natl. Acad. Sci. USA **95**, 9541-9546

7 Frohm, M., Agerberth, B., Ahangari, G., Stahle-Backdahl, M., Liden, S., Wigzell, H. and Gudmundsson, G. H. (1997) The expression of the gene coding for the antibacterial peptide LL-37 is induced in human keratinocytes during inflammatory disorders. J. Biol. Chem. **272**, 15258- 15263

8 Sorensen, O. E., Follin, P., Johnsen, A. H., Calafat, J., Tjabringa, G. S., Hiemstra, P. S. and Borregaard, N. (2001) Human cathelicidin, hCAP-18, is processed to the antimicrobial peptide LL-37 by extracellular cleavage with proteinase 3. Blood **97**, 3951–3959

9 Agerberth, B., Charo, J., Werr, J., Olsson, B., Idali, F., Lindbom, L., Kiessling, R., Jornvall, H., Wigzell, H. and Gudmundsson, G. H. (2000) The human antimicrobial and chemotactic peptides LL-37 and alpha-defensins are expressed by specific lymphocyte and monocyte populations. Blood **96**, 3086-3093

10 Bals, R., and Wilson, J. M. (2003) Cathelicidins-a family of multifunctional antimicrobial peptides. Cell Mol Life Sci **60**, 711-720

11 Bals, R., Wang, X., Wu, Z., Freeman, T., Bafna, V., Zasloff, M., Wilson, J.M. 1998 Human beta-defensin 2 is a salt-sensitive peptide antibiotic expressed in human lung. J Clin Invest.**102**, 874-880

12 Johansson, J., Gudmundsson, G.H., Rottenberg, M.E., Berndt, K.D., Agerberth, B. (1998) Conformation-dependent antibacterial activity of the naturally occurring human peptide LL-37. J Biol Chem. **273**, 3718-3724

13 Oren, Z., Lerman, J.C., Gudmundsson, G.H., Agerberth, B., Shai, Y. (1999) Structure and organization of the human antimicrobial peptide LL-37 in phospholipid membranes: relevance to the molecular basis for its non-cell-selective activity. Biochem J. **341**, 501-513

14 Zelezetsky, I., Pontillo, A., Puzzi, L., Antcheva, N., Segat, L., Pacor, S., Crovella, S., Tossi, A. (2006) Evolution of the primate cathelicidin. Correlation between structural variations and antimicrobial activity. J Biol Chem. **281**, 19861-19871

15 Yang, D., Chen, Q., Schmidt, A.P., Anderson, G.M., Wang, J.M., Wooters, J., Oppenheim, J.J., Chertov, O. (2000) LL-37, the neutrophil granule- and epithelial cell-derived cathelicidin, utilizes formyl peptide receptor-like 1 (FPRL1) as a receptor to chemoattract human peripheral blood neutrophils, monocytes, and T-cells. J Exp Med **192**, 1069-1074

16 Yang, D., Chertov, O., Oppenheim, J.J. (2001) Participation of mammalian defensins and cathelicidins in anti-microbial immunity: receptors and activities of human defensins and cathelicidin (LL-37). J Leukoc Biol. **69**, 691-697

17 Tjabringa, G.S., Aarbiou, J., Ninaber, D.K., Drijfhout, J.W., Sørensen, O.E., Borregaard, N., Rabe, K.F., Hiemstra, P.S. (2003) The antimicrobial peptide LL-37 activates innate immunity at the airway epithelial surface by transactivation of the epidermal growth factor receptor. J Immunol. **171**, 6690-6696

18 Herasimenka, Y., Benincasa, M., Mattiuzzo, M., Cescutti, P., Gennaro, R., Rizzo, R. (2005) Interaction of antimicrobial peptides with bacterial polysaccharides from lung pathogens. Peptides. **26**, 1127-1132

19 Wang, Y., Agerberth, B., Lothgren, A., Almstedt, A., Johansson, J. (1998) Apolipoprotein A-I binds and inhibits the human antibacterial/cytotoxic peptide LL-37. J. Biol. Chem. **273,** 33115–33118

20 Mennicke, U. and Salditt, T. (2002) Preparation of Solid-Supported Lipid Bilayers by Spin-Coating. Langmuir **18**, 8172-8177

21 Bechinger, B., Ruysschaert, J.M. and Erik Goormaghtigh (1999) Membrane Helix Orientation from Linear Dichroism of Infrared Attenuated Total Reflection Spectra. Biophysical Journal **76**, 552–563

22 Martin, Y., Williams, C. C. and Wickramasinghe, H. K. (1987) Atomic force microscope–force mapping and profiling on a sub 100-Å scale. J. Appl. Phys. **61**, 4723-4729

23 Ladokhin, A. S., Wimley, W. C., Hristova, K., and White, S. H. (1997) Mechanism of leakage of contents of membrane vesicles determined by fluorescence requenching. Meth Enzymol **278**:474-485

24 Chen, Y.H., Yang, J.T. and Chau, K.T. (1974) Determination of the helix and beta form of proteins in aqueous solution by circular dichroism. Biochmistry **13**, 3350-3359

25 Wagschal, K., Tripet, B. Lavigne, P. Mant, C., Hodges, R.S. (1999) The role of position a in determining the stability and oligomerization state of alpha-helical coiled coils: 20 amino acid stability coefficients in the hydrophobic core of proteins. Protein Sci. **8**, 2312-2329

26 Chirgadze, Y.N., Fedorov, O.V., Trushina, N.P. (1975) Estimation of amino acid residue side chain absorption in the infrared spectra of protein solutions in heavy water. Biopolymers **14**, 679–694

27 Venyaminov, S.Y., Kalnin, N.N. (1990) Quantitative IR spectrophotometry of peptide compounds in water (H2O) solutions. I. Spectral parameters of amino acid residue absorption bands. Biopolymers **30**, 1243–1257

28 Rahmelow, K., Hu¨bner, W., Ackermann, T. (1998) Infrared absorbances of protein side chains. Anal. Biochem. **257**, 1–11

29 Tamm L. and. Tatulian, Infrared spectroscopy of proteins and peptides in lipid bilayers (1997)Quarterly Reviews of Biophysics 30, 4 pp. 365–429. Cambridge University Press

30 Braiman, M. S., Briercheck, D. M. and Kriger, K. M. (1999) Modeling Vibrational Spectra of Amino Acid Side Chains in Proteins: Effects of Protonation State, Counterion, and Solvent on Arginine C-N Stretch Frequencies. J. Phys. Chem. **103**, 4744-4750

31 Martinez, G., Millhause, G. (1995) FTIR spectroscopy of alanine-based peptides: assignment of the amide I' modes for random coil and helix. J Struct Biol. **114**, 23-27

32 Silvestro, L., and Axelsen, P. H. (1998) Infrared spectroscopy of supported lipid monolayer, bilayer, and multibilayer membranes. Chem Phys Lipids **96**, 69-80

33 Hallock, K.J. Lee, D.K. and Ramamoorthy, A. (2003) MSI-78, an analogue of the magaininantimicrobial peptides, disrupts lipid bilayer structure via positive curvature strain. Biophys. J. **84,** 3052–3060

34 Matsuzaki, K., Mitani, Y., Akada, K.Y., Murase, O., Yoneyama, S., Zasloff, M. and Miyajima, K. (1998) Mechanism of synergism between antimicrobial peptides magainin 2 and PGLa. Biochemistry **37,** 15144–15153

35 Yang, L. Harroun, T.A. Weiss, T.M. Ding, L. Huang, H.W. (2001) Barrel-stave model or toroidal model? A case study on melittin pores. Biophys. J. **81**, 1475–1485.

36 Park ,S.C, Kim, J.Y, Shin, S.O., Jeong, C.Y., Kim, M.H., Shin, S.Y., Cheong, G.W., Park, Y., Hahm, K.S. (2006) Investigation of toroidal pore and oligomerization by melittin using transmission electron microscopy. Biochem Biophys Res Commun. **343**(1),222-228

37 Wildman, K. A., Lee, D. K., Ramamoorthy, A. (2003) Mechanism of Lipid Bilayer Disruption by the Human Antimicrobial Peptide, LL-37. Biochemistry **42**, 6545-6558

38 Tossi, A., Tarantino, C. and Romeo, D. (1997) Design of synthetic antimicrobial peptides based on sequence analogy and amphipathicity. Eur. J. Biochem. **250**, 549-558

39 Zasloff, M. (2002) Antimicrobial peptides of multicellular organisms. Nature **415**, 389-395

40 Pag, U., Oedenkoven, M., Sass, V., Shai, Y., Shamova, O., Antcheva, N., Tossi, A., Sahl, H.G. (2008) Analysis of in vitro activities and modes of action of synthetic antimicrobial peptides derived from an alpha-helical 'sequence template'. J Antimicrob Chemother. **61**, 341-352

41 Porcelli, F., Verardi, R., Shi, L., Henzler-Wildman, K.A., Ramamoorthy, A., Veglia, G. (2008) NMR structure of the cathelicidin-derived human antimicrobial peptide LL-37 in dodecylphosphocholine micelles. Biochemistry. **47**, 5565-557

42 Tomasinsig L., Pizzirani, C., Skerlavaj, B., Pellegatti, P., Gulinelli, S., Tossi, A., Di Virgilio, F., Zanetti, M. (2008) The human cathelicidin LL-37 modulates the activities of the P2X7 receptor in a structure-dependent manner. J Biol Chem. (*Epub ahead of print*).

43 Zelezetsky, I., Pacor, S., Pag, U., Papo, N., Shai, Y., Sahl, H.G., Tossi, A. (2005) Controlled alteration of the shape and conformational stability of alpha-helical cell-lytic peptides: effect on mode of action and cell specificity. Biochem J. **390**, 177-188

TABLES and FIGURES

Table 1: Sequence and physico-chemical properties of LL-37 orthologues

peptide	sequence*	MW	q†	<H>‡	μH‡	attractions§ / repulsions
LL-37	LLGDFFRKSKEKIGKEFKRIVQRIKDFLRNLVPRTES	4493	+6	-1.83	0.59	9/7
*ppy*LL-37	LLGDFFRKAREKIGEEFKRIVQRIKDFLRNLVPRTES	4506	+4	-1.70	0.59	11/5
*mmu*RL37	RLGNFFRKVKEKIGGGLKKVGQKIKDFLGNLVPRTAS	4101	+8	-1.66	0.56	4/5

*Conserved residues in orthologues relative to human LL-37 are shaded grey
†Charge
‡Mean hydrophobicity and relative hydrophobic moment, calculated as described in [14]
§ Derived from Fig. 6 in [14]

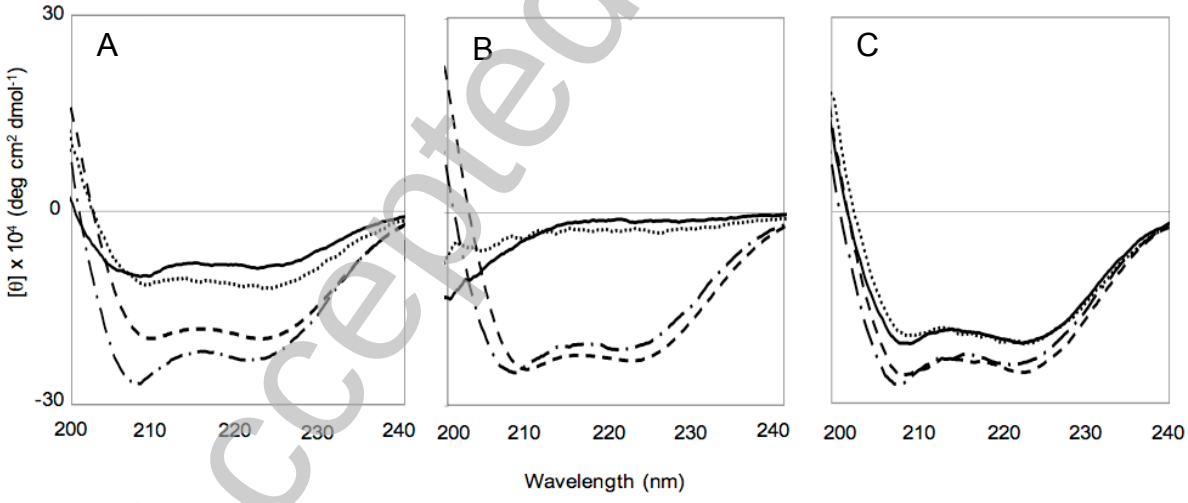

Figure 1 CD spectra of LL-37 orthologues

LL37(A), *mmu*RL37 (B) and *ppy*LL-37 (C) in presence of phosphate buffer (PBS) (——), 50% TFE (– · –), PG/dPG (---) and PC/SM/Ch (·····) LUVs. Peptide [20μM] and lipid [400 μM lipids] in PBS.

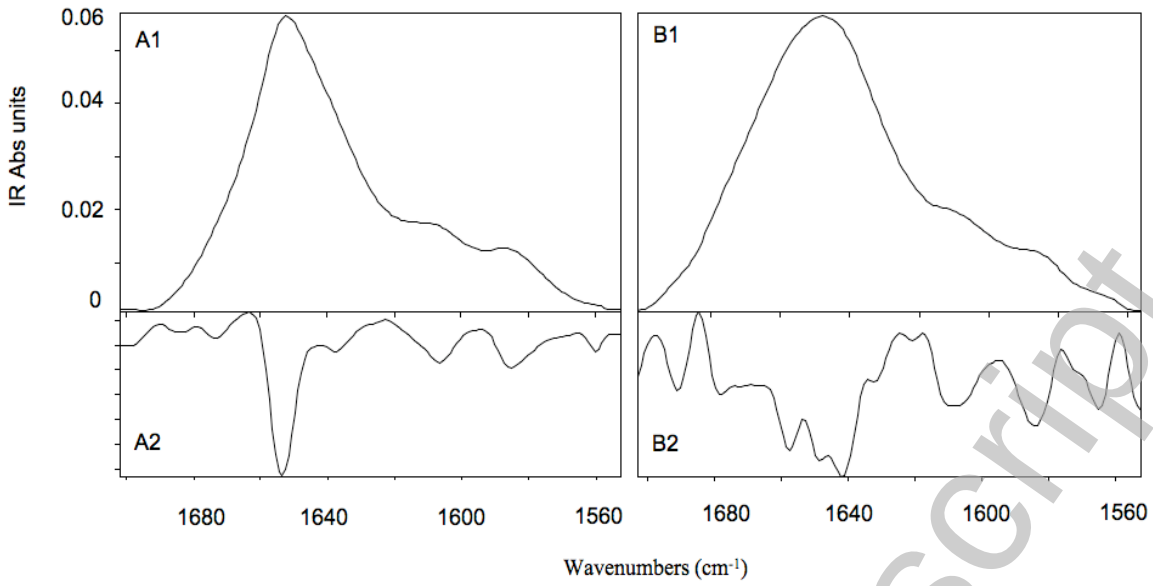

Figure 2 FTIR transmission spectra of LL-37 and *mmu*RL37 in deuterated water

FTIR amide I' spectra of LL37 (A1) and mmuRL37 (B1) in deuterated water [2mM peptide concentration], after complete H/D exchange. The bottom panels show the respective 2nd derivatives (A2, B2).

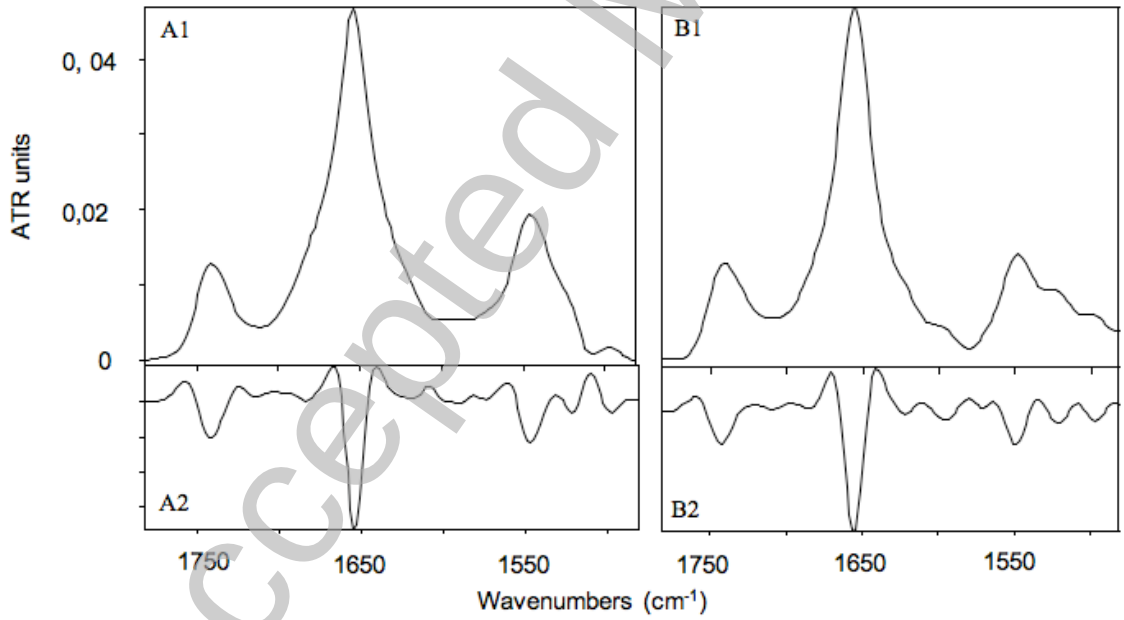

Figure 3 ATR-FTIR spectra of LL37 and *mmu*RL37 in lipid bilayers

Amide I and II spectra of LL-37 (A) and *mmu*RL37 (B) in a supported PG bilayer in dehydrated conditions (estimated P/L ratio 1:20). In panels A&B2 the respective amide I and II 2nd derivatives are shown.

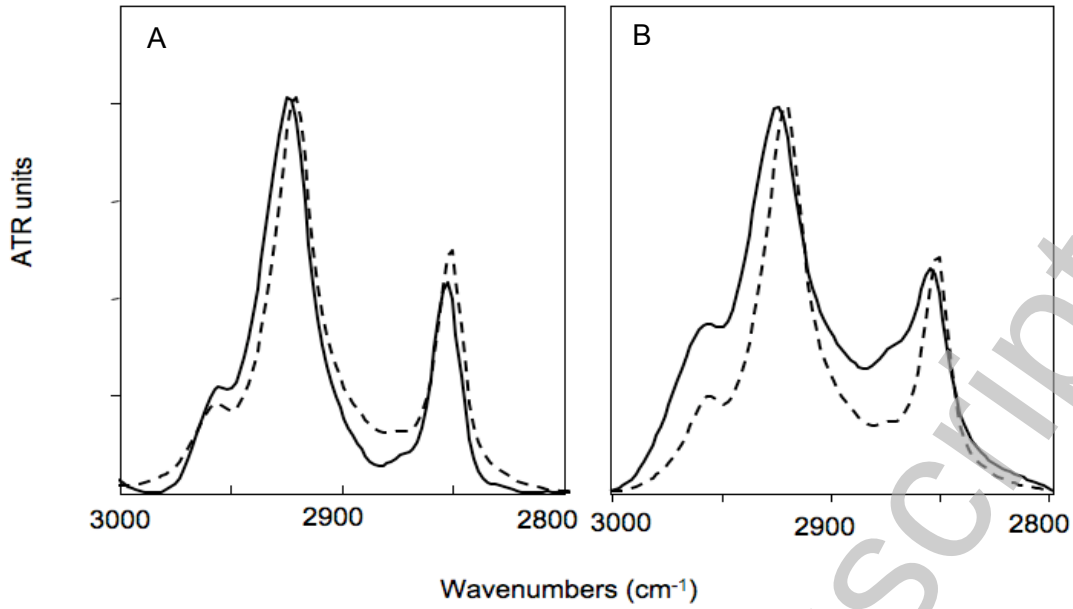

Figure 4 ATR-FTIR spectra for lipid acyl chains

Spectra for lipid acyl chain CH_2 stretching IR bands of dehydrated supported PG bilayer, before (---) and after (—) interaction with LL-37 (A) and *mmu*RL37 (B).

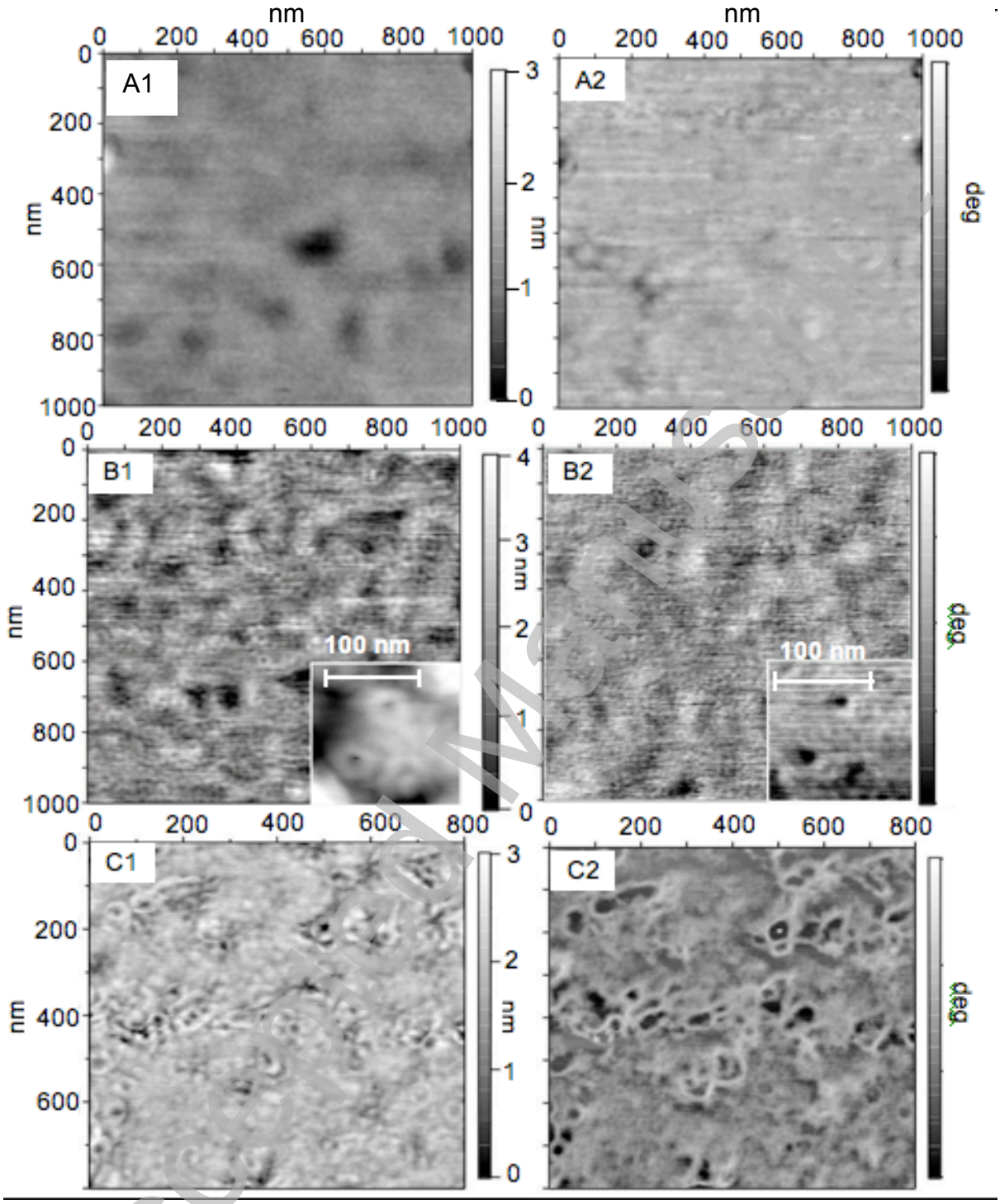

Figure 5 AFM images of supported PG bilayers in the presence of LL-37 or *mmu*RL-37

AFM topographic (A1, B1, C1) and phase (A2, B2, C1) images of the lipid bilayer without peptide (A1, A2) and upon interaction with LL-37 (A1, A2), and *mmu*RL37 (B1, B2), (1:20 P/L estimated

ratio). Insets are respectively the topography and phase images at a higher resolution of the lipid bilayer upon LL-37 interaction.

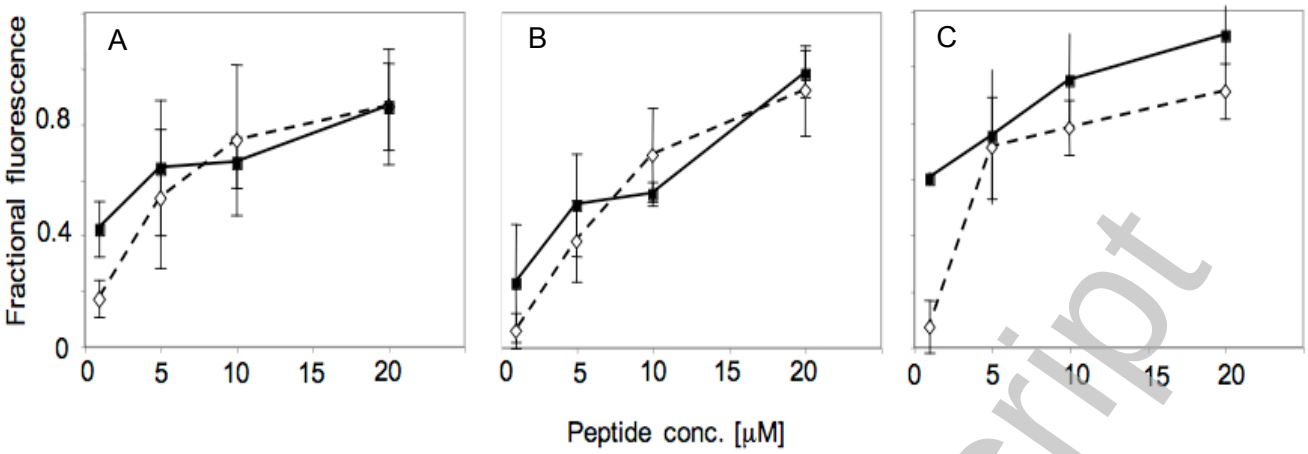

Figure 6 Permeabilization of LUVs in the presence of LL-37 orthologues

A-C) ANTS/DPX leakage from anionic and neutral LUVs in the presence of different peptide concentrations. ANTS fractional fluorescence due to permeabilization of (--◇--) PG/dPG (95:5) LUVs, and (—■—) of PC/SM/Ch (40:40:20) LUVs [300μM lipid], exerted by LL-37 (A), *mmu*RL37 (B), *ppy*LL-37 (C) at different peptide concentrations.

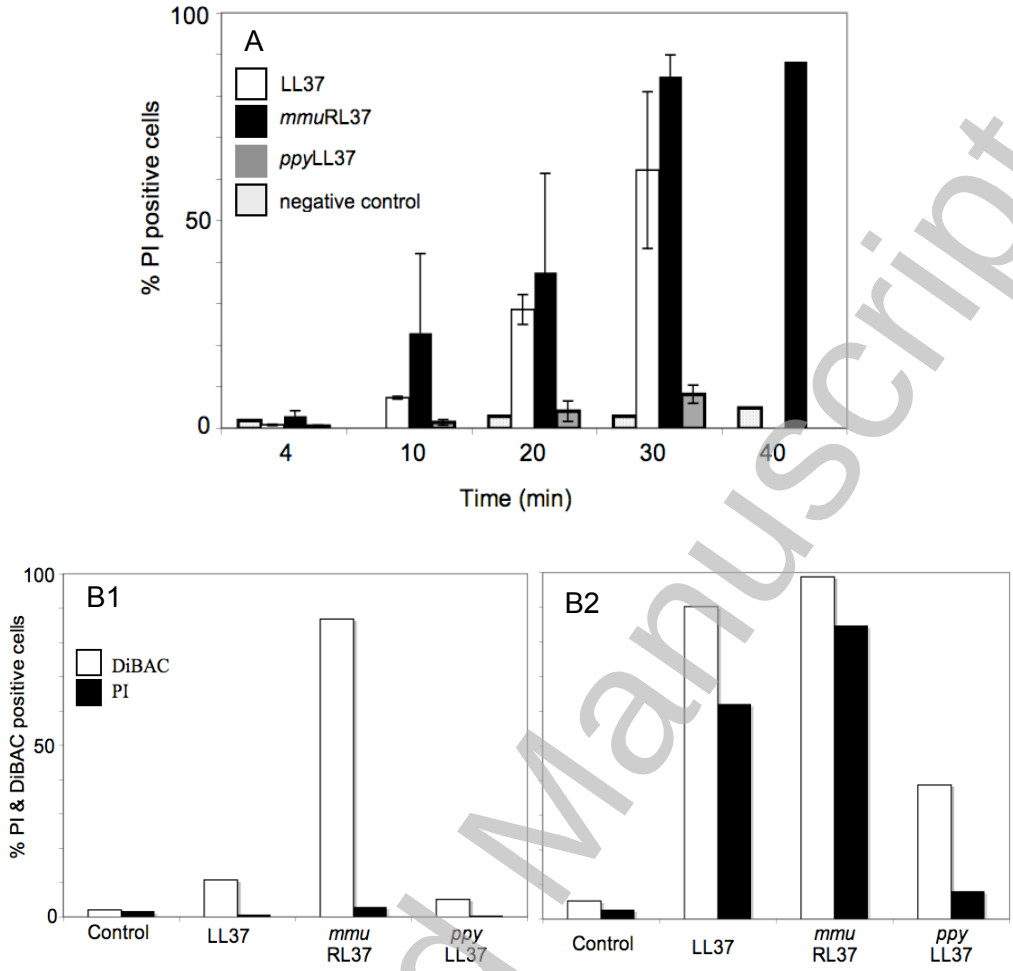

Figure 7 Permeabilization and depolarization of *E.coli* ML35 cells investigated by flow cytometry

A) % PI positive *E.coli* ML35 cells after exposure to the indicated peptides for different times; B1) % PI and % DiBAC positive *E.coli* ML35 cells at minute 4 (1B) and minute 30 (B2) after exposure to peptides. Peptide concentration 0,1 μM, 10^6 CFU/ml *E.coli* in PBS, 37°C.

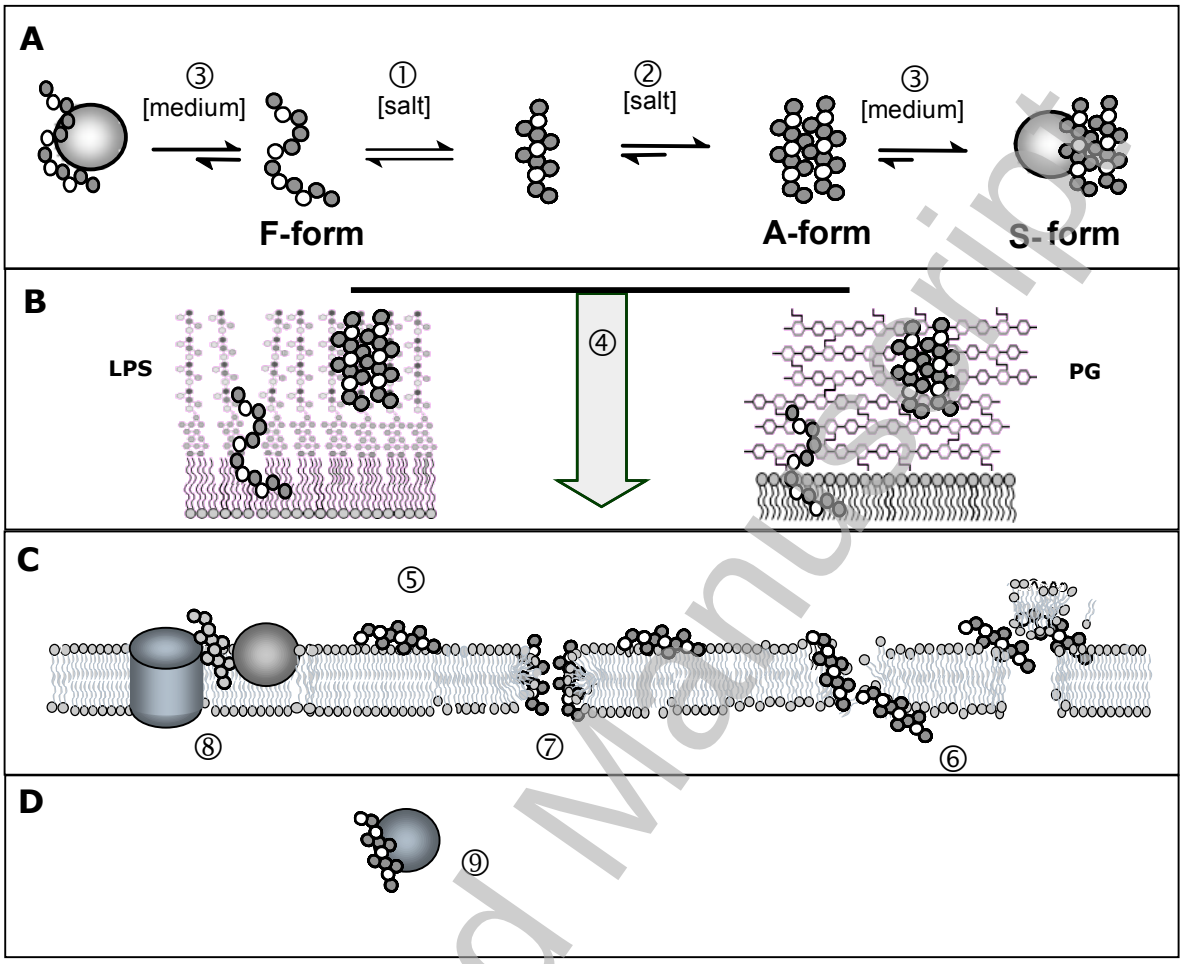

Figure 9 General model for the modes of action of a helical AMP.

AMPs reach the microbial surface from bulk solution (layer A), by crossing the outer cell-wall components (layer B) so that they can interact with the cytoplasmic membrane (layer C) and possibly translocate into the cytoplasm (layer D). In bulk solution they are in equilibrium between unstructured and conformational ① or aggregational ② forms, and can also bind non-productively to serum or interstitial components or bacterial exopolisaccharides ③. The different forms modulate interaction with outer membrane (LPS) or peptidoglycan (PG) components ④. At the membrane surface, interaction consists of an initial surface electrostatic binding ⑤ followed by insertion, membrane compromising and cellular inactivation by one or more of several possible mechanisms ⑥-⑨ (see text). F-, A-, and S- forms refer respectively to unstructured/monomeric (Free), structured/oligomeric (Aggregated) and medium-bound (Segregated) forms.